

Anisotropic turbulence in weakly stratified rotating magnetoconvection

A. Giesecke¹

¹*Astrophysikalisches Institut Potsdam, An der Sternwarte 16, D-14482 Potsdam, Germany*

Accepted 1999 November 11. Received 1999 October 6; in original form 1999 August 3

SUMMARY

Numerical simulations of the 3D MHD-equations that describe rotating magnetoconvection in a Cartesian box have been performed using the code NIRVANA. The characteristics of averaged quantities like the turbulence intensity and the turbulent heat flux that are caused by the combined action of the small-scale fluctuations are computed. The correlation length of the turbulence significantly depends on the strength and orientation of the magnetic field and the anisotropic behavior of the turbulence intensity induced by Coriolis and Lorentz force is considerably more pronounced for faster rotation. The development of isotropic behavior on the small scales – as it is observed in pure rotating convection – vanishes even for a weak magnetic field which results in a turbulent flow that is dominated by the vertical component. In the presence of a horizontal magnetic field the vertical turbulent heat flux slightly increases with increasing field strength, so that cooling of the rotating system is facilitated. Horizontal transport of heat is always directed westwards and towards the poles. The latter might be a source of a large-scale meridional flow whereas the first would be important in global simulations in case of non-axisymmetric boundary conditions for the heat flux.

Key words: magnetoconvection – anisotropic turbulence – geodynamo – turbulent heat flux – MHD-simulations

1 INTRODUCTION

Anisotropic turbulence is a fundamental feature in many astro- or geophysical systems. Well known realizations are the turbulent motions in the solar convection zone or the flow of liquid iron in the outer core of the Earth. Both kinds of convectively driven flows are assumed to be responsible for dynamo action. Flow and field are attuned in a complex non-linear system where the flow produces the magnetic field which in turn backreacts on the field producing flow. Direct observations of the sun offer the possibility to examine the details of the complicated interactions between convection and magnetic fields. On the top of the solar convection zone, in the photosphere, where rotational effects are rather unimportant, occasionally strong localized and radial oriented magnetic fields inhibit the convective transport of energy which results in a cooler (and therefore darker) area, a sunspot (see e.g. Weiss, 1990). Numerical simulations of non-linear magnetoconvection confirm that a vertical magnetic field suppresses turbulent motions as well as it considerably reduces the size of the convection cells, a result that has been known from the linear stability analysis of Chandrasekhar (1961). The smaller cells come along with reduced variations of the temperature so that the correlations of velocity and temperature fluctuations, the turbulent heat flux, de-

crease with increasing field (Cattaneo et al., 2003). Towards the edge of the sunspot the field changes its orientation to a more horizontal direction. As a result the flow pattern changes to small brighter and darker elongated filaments that surround the sunspot (Weiss et al., 2004). Thermodynamic properties like the heat transport and the temperature distribution are undoubtedly linked to the anisotropy induced by the dominant magnetic field component. Closely related to the interaction of convection, magnetic field and turbulent heat transport are questions about the existence of warmer (and therefore brighter) rings around sunspots (Eschrich & Krause, 1977; Rüdiger & Kitchatinov, 2000) or the behavior of (star-) spots in fast rotating stars. In contrast to the sun, observations of fast rotating stars using Doppler-Imaging techniques reveal an accumulation of star spots close to the poles (Strassmeier, 2002, 2006). This phenomenon clearly indicates the different behavior of convectively driven turbulence in fast rotating objects and points out that a different dynamo mechanism is running where differential rotation is of minor importance (Bushby, 2003). Comparable considerations might also be of interest for the Earth because observations of the radial field component at the core mantle boundary as well as highly resolved simulations of the geodynamo show strong localized flux patches

whose pattern and pair-like occurrence resemble the behavior of sunspots (Roberts & Glatzmaier, 2000; Jackson, 2003).

However, the particular properties of a fast rotating planetary body like the Earth lead to physical conditions that differ significantly from the sun or stellar objects. A small density contrast between the top and the bottom of the fluid outer core and a nearly incompressible fluid result in a small Mach number flow which is essentially influenced by the non-linear back-reaction of a strong magnetic field. Convection in the fluid outer core is mainly affected by two dominant forces, the Lorentz force due to the strong magnetic field and the Coriolis force due to the fast rotation of the Earth. In such a rapidly rotating convection driven dynamo the turbulence is subject to three preferred directions defined by magnetic field, rotation axis and gravity. The arising anisotropies result in a plate like form of convection cells which are aligned along the rotation axis and elongated in the direction of the dominant magnetic field component (Braginsky & Meytlis, 1990; St. Pierre, 1996; Matsushima et al., 1999).

Despite the progress in computational and numerical techniques that have been made during the recent years, it is still impossible to simulate turbulent convection in rotating spherical shells with a sufficient resolution so that the resolved scale range of the turbulence is rather restricted (Hollerbach, 2003). Furthermore, anisotropy usually is neglected by an implicit assumption of a large eddy simulation where scalar parameters resemble the turbulent values of the diffusivities. Beside the fact that mostly the diffusivities – for the reason of numerical stability – have to be chosen much larger than even the (poorly known) “real” turbulent values, this oversimplifying assumption describes an isotropic transport of flux and an isotropic dissipation of energy. This is only justified if either the resolution is high enough so that all dynamical important modes are resolved or if no preferred direction originated by external forces, stratification or boundary conditions exists. Both, in general, are not the case. In order to include anisotropic effects in a more sophisticated way, turbulence models have to be considered where tensorial expressions for the diffusivities take care of the directional dependence of the turbulence and the influence of the unresolved scales is parameterized in terms of the resolved large-scale fields.

Tensor coefficients for the viscous and thermal diffusivity of a fast rotating and a strong field model of the Earth’s core have been derived by Phillips & Ivers (2001, 2003). They present expressions that describe enhanced diffusion along a dominant azimuthal magnetic field. Non-diagonal elements are neglected so that diffusion in the horizontal directions due to a coupling between vertical and horizontal components of the turbulent flow is not included. The results are intended for the use in pseudo-spectral codes but at this stage no applications in numerical investigations are available so that the consequences for global simulations remain unknown.

A different approach is examined by Buffett (2003) and Matsushima (2004, 2005). They present a subgridscale (SGS) model which is essentially based on the self-similarity of the turbulence. By comparison of a highly resolved direct numerical simulation (DNS) with a large eddy simulation based on the SGS model, they show that the SGS model is able to predict appropriate anisotropic heat- and momentum

fluxes. An advanced version of the SGS model that includes the Lorentz- and induction terms is introduced by Matsui & Buffett (2005). They apply the so called non-linear gradient model, an adaption of the similarity model that additionally is based on the local character of the turbulence. In general, the SGS models coincide rather well with the direct numerical simulations, however, both models are not able to reproduce all details of the spatiotemporal behavior. Furthermore, systematic deviations are obtained in mean quantities, like kinetic and magnetic energy, which are situated between the values from the resolved DNS and the values of a truncated, unresolved DNS.

In order to evaluate the functionality of SGS models it is useful to further investigate the development of a convectively driven turbulence in view of the dependence on field strength and latitude. Subject matter of the present paper is the connection between turbulence characteristics, that are caused by the average action of the small-scale fluctuations and the turbulent transport of heat which may essentially contribute to the conditions that determine the temperature distribution within the fluid outer core. A simplified Cartesian system is examined where a convectively driven turbulence in a conducting fluid is subject to fast rotation and an externally imposed magnetic field. As we do not intend to reproduce geophysical realities in all details, the presented investigation is based on a highly idealized system where the emphasis lies on the anisotropy inducing effects of rotation and magnetic field. Properties like the exact behavior of the temperature gradient, the equation of state or the influence of curvature are assumed to be of secondary importance.

2 THE MODEL

2.1 General properties

A detailed description of the applied local model can be found in Giesecke et al. (2005). Figure 1 shows a sketch of the computational domain, a Cartesian box placed somewhere on a spherical shell at a co-latitude θ . The unit vectors \hat{x} , \hat{y} , \hat{z} form a right-handed co-rotating Cartesian coordinate system with \hat{x} pointing towards the equator, \hat{y} pointing in the toroidal direction (from west to east) and \hat{z} pointing from the bottom to the top of the box. In global spherical coordinates, \hat{z} represents the radial direction \hat{r} (oriented from inside to outside), \hat{y} the azimuthal direction $\hat{\varphi}$ (oriented eastwards) and \hat{x} the meridional direction $\hat{\theta}$ (oriented towards the equator). The angular velocity Ω in the co-rotating local box coordinate system is given by $\Omega = -\Omega \sin \theta \hat{x} + \Omega \cos \theta \hat{z}$ where Ω is the angular velocity of the rotating spherical shell. The box with an aspect ratio 8:8:1 is placed at different latitudes on the northern hemisphere of the rotating spherical shell and a standard resolution of $100 \times 100 \times 80$ grid points is used in all calculations. The co-latitude angle θ is varied from $\theta = 0^\circ$ (north pole) to $\theta = 75^\circ$.

2.2 Equations

The MHD-equations for a rotating fluid, including the effects of thermal conduction, compressibility, viscous friction and

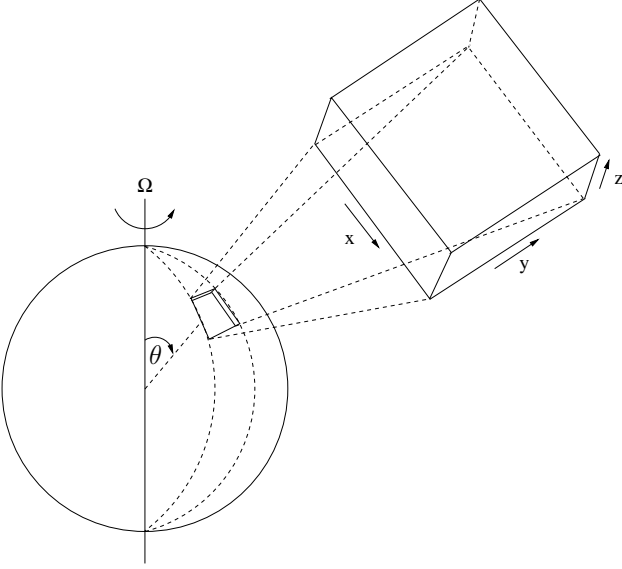


Figure 1. Model box as part of a rotating spherical shell at co-latitude θ .

losses due to magnetic diffusivity, are

$$\partial_t \rho = -\nabla \cdot (\rho \mathbf{u}), \quad (1)$$

$$\begin{aligned} \partial_t (\rho \mathbf{u}) &= -\nabla \cdot (\rho \mathbf{u} \mathbf{u}) - \nabla p + \nabla \cdot \sigma + \rho \mathbf{g} \\ &\quad + \frac{1}{\mu_0} (\nabla \times \mathbf{B}) \times \mathbf{B} - 2\rho \boldsymbol{\Omega} \times \mathbf{u}, \end{aligned} \quad (2)$$

$$\begin{aligned} \partial_t e &= -\nabla \cdot (e \mathbf{u}) - p \nabla \cdot \mathbf{u} + \sigma \cdot \nabla \mathbf{u} + \frac{\eta}{\mu_0} |\nabla \times \mathbf{B}|^2 \\ &\quad + \nabla \cdot (\kappa \nabla T), \end{aligned} \quad (3)$$

$$\partial_t \mathbf{B} = \nabla \times (\mathbf{u} \times \mathbf{B} - \eta \nabla \times \mathbf{B}). \quad (4)$$

Here, ρ denotes the density, \mathbf{u} the velocity, p the pressure, \mathbf{B} the magnetic flux density, T the temperature and e the thermal energy density. A constant gravitational field $\mathbf{g} = -g\hat{\mathbf{z}}$ is assumed within the domain. The viscous stress tensor σ is given by $\sigma_{ij} = \nu\rho(\partial_j u_i + \partial_i u_j - 2/3\nabla \cdot \mathbf{u}\delta_{ij})$. ν denotes the kinematic viscosity and κ the thermal conductivity coefficient. The values of κ , the dynamic viscosity $\nu_{\text{dyn}} = \nu\rho$ and the magnetic diffusivity η are constant within the box volume. An ideal gas equation of state is assumed:

$$p = (\gamma - 1)e = \frac{k}{m\bar{\mu}}\rho T \quad (5)$$

where k is the Boltzmann constant, m the atomic mass unit, $\bar{\mu}$ the mean molecular weight ($\bar{\mu} = 1$ for all runs) and $\gamma = c_p/c_V = 5/3$ is the ratio of c_p , the specific heat at constant pressure, and c_V , the specific heat at constant volume. The permeability μ_0 is given by the vacuum value $\mu_0 = 4\pi \times 10^{-7} \text{VsA}^{-1}\text{m}^{-1}$.

The equations (1) – (4) are solved applying the code NIRVANA (Ziegler 1998, 1999). NIRVANA makes use of a dimensional- and operator splitting approach. A second-order accurate finite-volume scheme with a piecewise linear reconstruction and monotized slope limiter (van Leer) is used for the hydrodynamic advection part of the equations. A constraint transport solver utilizing the method of characteristics is employed for the numerical solution of the induction equation. The time integration of the source terms is

performed by an explicit Euler scheme (except the Coriolis force which is treated analytically).

2.3 Initial state and input parameters

The simulations are started with an initial state that is determined by a hydrostatic equilibrium $\partial_z p = -\rho g$ and a polytropic temperature distribution $T = T_0 (\rho/\rho_0)^\Gamma$ in the absence of motions (the subscript 0 refers to values taken at the top boundary of the box). With the equation of state (5) the initial density distribution is given by

$$\rho(z) = \rho_0 \left(1 + \frac{dT/dz}{T_0} (d - z) \right)^{1/\Gamma}, \quad (6)$$

where d stands for the vertical box extension and the polytropic index Γ is given by $\Gamma = \ln(1 + d \frac{dT/dz}{T_0}) / \ln \xi$. The stratification index $\xi = \rho_{\text{bot}}/\rho_0$, the temperature T_0 and the global temperature gradient dT/dz are prescribed input parameters.

The parameters ν, κ and η are calculated from the Rayleigh number Ra,

$$\text{Ra} = \frac{c_p d^4 \rho g}{\kappa \nu T} \left(\frac{dT}{dz} - \frac{g}{c_p} \right) \quad (7)$$

with $c_p = k(m\bar{\mu})^{-1}\gamma(\gamma - 1)^{-1}$ the specific heat at constant pressure, the Prandtl number $\text{Pr} = \nu\rho c_p/\kappa$ and the magnetic Prandtl number $\text{Pm} = \nu/\eta$. The basic parameter set used for all simulations that are presented in this paper is given by $\text{Ra} = 10^6$, $\text{Pr} = 0.5$ and $\text{Pm} = 0.5$. The diffusivity parameters are scalar quantities assuming that in the local model the resolved scales contain most of the energy, so that the anisotropic transport is described with sufficient accuracy and the remaining non-resolved modes are less important. The rotation rate Ω is parameterized by the Taylor number given by

$$\text{Ta} = \frac{4\Omega^2 d^4}{\nu^2} \quad (8)$$

which is related to the Ekman number by $\text{Ta} = \text{Ek}^{-2}$. Essentially, a rotating system is examined where Ta is set to a value of 10^7 . A few simulations with a Taylor number $\text{Ta} = 10^6$ have been performed which demonstrate the significant changes in the behavior of the turbulence as the rotation rate increases.

The magnetic field is expressed by the Elsässer number:

$$\Lambda = \frac{\mathbf{B}^2}{2\Omega\mu_0\rho\eta}. \quad (9)$$

Λ represents the relation of the Lorentz force to the Coriolis force, which are assumed to be of the same order of magnitude within the fluid outer core. The original picture favors $\Lambda \approx O(1)$ because at this value the critical Rayleigh number Ra_{crit} at which the onset of thermal convection occurs, becomes minimal. In that case the Coriolis force can be balanced by the Lorentz force. Then, there remains no need for balancing these terms with the (extremely small) viscous terms which would force the convection to occur on very short length scales. Such a flow would be much more difficult to maintain which is evident on the basis of the suppression of convective motions in simple rotating convection or non-rotating magnetoconvection. For a detailed

description of the underlying mechanism see e.g. Rüdiger & Hollerbach (2004). However, Zhang & Jones (1994) did not find such a minimum for convection in a rotating spherical shell, but they were able to show that the existence of a stable magnetic field requires an Elsässer number in the range $1 \lesssim \Lambda \lesssim 10$.

For the comparison of the magnetic quenching character in simulations with different rotation rates, Λ is not a suitable parameterization of the field strength. For that case, the dependence on the imposed field strength is expressed in units of the equipartition field strength B_{eq} defined by

$$B_{\text{eq}} = \sqrt{\mu_0 \rho} u_{\text{rms}}, \quad (10)$$

where u_{rms} denotes the root-mean-square velocity (see definition in the following section) for non-rotating and non-magnetic convection (in code units: $u_{\text{rms}} \approx 19.5$).

2.4 Averaging procedure

Due to the small stratification all considered quantities do only weakly depend on the vertical coordinate z (except close to the upper and the lower boundaries). Therefore it is justified to characterize the turbulence properties of a fluctuating quantity by a volume average given by

$$\langle f' \rangle = \frac{1}{N} \sum_{i,j,k} \underbrace{\left(f_{i,j,k}(t) - \bar{f}_z(t) \right)}_{f'_{i,j,k}}. \quad (11)$$

On the left hand side, f' represents a fluctuating quantity and the brackets $\langle \cdot \rangle$ denote the averaging procedure. On the right hand side, $f_{i,j,k}(t)$ represents the numerically computed value of the quantity f at a certain grid cell labeled by i, j, k at a certain time t . $\bar{f}_z(t)$ represents the horizontal average of the considered quantity. $N = n_x n_y n_z$ denotes the number of grid cells used for averaging. Time averaging is done for periods with no significant changes in the statistically steady convection state. Convergence of the time-averaged solutions has been checked by comparing results obtained from averages over different (increasing) periods. Reasonable results are obtained for averaging periods larger than at least 20 turnover times $\tau_{\text{adv}} = d/u_{\text{rms}}$, where the root mean square velocity u_{rms} is defined as $u_{\text{rms}} = \sqrt{\langle \mathbf{u}'^2 \rangle}$.

All quantities show fluctuations in time with a standard deviation of the order of 10 percent of their mean value. These fluctuations become smaller for increasing field strength, but within the context of this paper they do not exhibit any essential features so that the standard deviations are omitted for the reason of clarity.

2.5 Boundary Conditions

All quantities are subject to periodic boundary conditions in the horizontal directions. At the top and at the bottom of the computational domain constant values for density and temperature are imposed. The vertical boundary condition for the magnetic field is a perfect conductor condition, and a stress-free boundary condition is adopted for the horizontal components of the velocity u_x and u_y . Impermeable box walls at the top and the bottom lead to a vanishing u_z at the vertical boundaries. Table 1 summarizes the boundary

Table 1. Vertical boundary conditions

	ρ	T	\mathbf{u}	\mathbf{B}
top ($z = d$)	1	1	$\partial_z u_x = 0$ $\partial_z u_y = 0$ $u_z = 0$	$\partial_z B_x = 0$ $\partial_z B_y = 0$ $B_z = 0$
bottom ($z = 0$)	1.1	2	$\partial_z u_x = 0$ $\partial_z u_y = 0$ $u_z = 0$	$\partial_z B_x = 0$ $\partial_z B_y = 0$ $B_z = 0$

conditions and gives the initial values for density and temperature which describe the overall stratification and the global temperature gradient. For all simulations, temperature and density at the top of the box are scaled to unity, as it is the case for the global temperature gradient dT/dz and the box height d . A stratification index of $\xi = \rho_{\text{bot}}/\rho_0 = 1.1$ is used.

The boundary conditions certainly influence the behavior of the flow within the computational domain. To reduce the undesired effects of the boundaries all volume averages are performed over the inner part of the computational domain (between $z = 0.2$ to 0.8). Naturally, such a simplifying box model is not able to represent the large scale flows that may occur in a rotating sphere. Especially the existence of periodic boundary conditions in the horizontal directions filters out the fraction of the solution with wavelengths larger than the horizontal extension of the box (of course, this behavior is desired, because here only the small scale fluctuations are of interest). However, such filtering is not possible in the vertical direction due to the existence of density stratification and temperature gradient.

3 RESULTS

3.1 Convection pattern and anisotropy

Within the applied parameter regime all simulations result in a pressure dominated ($\beta = 2\mu_0 p/B^2 \gg 1$) low Mach number flow ($\text{Ma} = u_{\text{rms}}/c_s \ll 1$, with the sound speed $c_s = \sqrt{kT_0/m\bar{\mu}}$). Depending on rotation rate and field strength Ma is of the order of 10^{-2} (e.g. for $\Lambda = 1$ and $\text{Ta} = 10^7$ the characteristic Mach number is given by $\text{Ma} \approx 0.03$). The corresponding Reynolds numbers $\text{Re} = u_{\text{rms}}d/\nu$ are of the order of 100. The results that are presented in the following are obtained from simulations with an imposed horizontal field (B_y) which corresponds to a toroidal field in spherical coordinates. The typical structures of the convective motions are visualized in Fig. 2. The upper row presents the vertical velocity pattern obtained from a simulation run with $\text{Ta} = 10^6$ (left: $\Lambda \approx 1$ respectively $B = 0.1B_{\text{eq}}$, right: $\Lambda \approx 4$, respectively $B = 0.2B_{\text{eq}}$). The lower row presents the case $\text{Ta} = 10^7$ (left: $\Lambda \approx 1$ respectively $B = 0.2B_{\text{eq}}$, right: $\Lambda \approx 4$, respectively $B = 0.4B_{\text{eq}}$). All plots show a time snapshot of the vertical velocity pattern from a simulation run at $\theta = 45^\circ$.

The cell-like objects represented by the volume rendered iso-surfaces indicate coherent large-scale structures which span the full vertical extend of the domain. These convection cells are continuously formed, rearranged and dissolved leading to a quasi-stationary turbulent pattern which is more

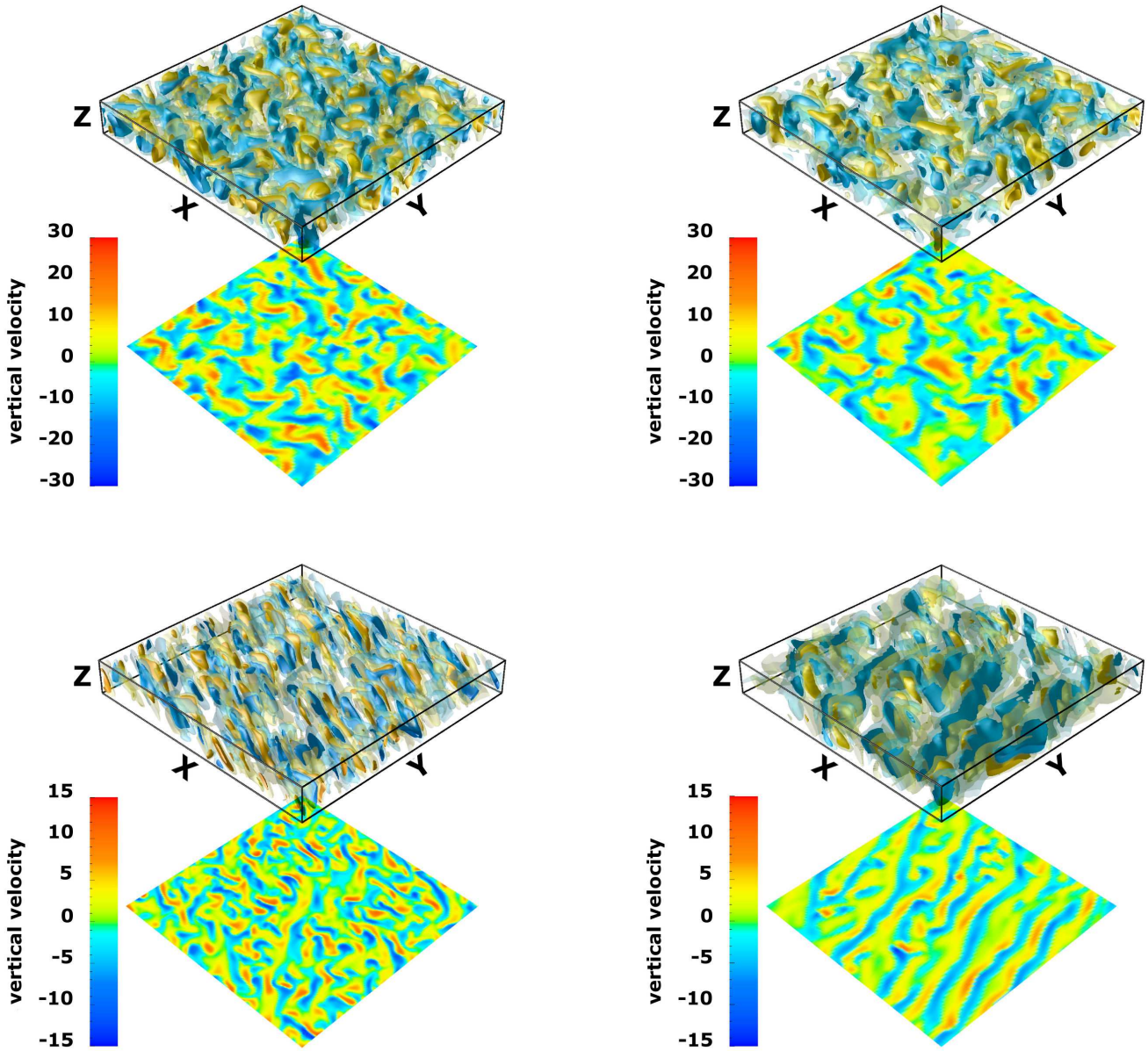


Figure 2. z -component of the velocity for $Ta = 10^6$ (upper row) and $Ta = 10^7$ (lower row). Left side: $\Lambda = 1$, right side: $\Lambda = 4$. All plots present a snapshot at $\theta = 45^\circ$. The solid iso-surfaces denote the vertical velocity at $u_z = u_{\text{rms}}$, and the transparent iso-surfaces denote the pattern at $u_z = 0.5u_{\text{rms}}$ (upper left $u_{\text{rms}} \approx 11.5$, upper right: $u_{\text{rms}} \approx 10.8$, lower left: $u_{\text{rms}} \approx 5.4$, lower right: $u_{\text{rms}} \approx 4.7$, all numbers in code units). A horizontal cut of the velocity field at a depth $z = 0.5$ is projected on a plane below the three dimensional box. Blue (dark) tones represent downwards oriented flow and yellow/red (light) colors represent upwards oriented flow.

irregular in the interior of the domain. According to the Taylor-Proudman theorem the convection cells are aligned with the rotation axis. The average horizontal size of the cells strongly depends on the rotation rate as well as the magnetic field strength and direction. The cell size is reduced for an increasing rotation rate and if the horizontal magnetic field exceeds a certain threshold the cells become elongated in direction of the dominant magnetic field component. With respect to Fig. 2 this is only noticeable in the faster rotating case whereas for $Ta = 10^6$ the convection

pattern remains nearly unaffected as the Elsässer number is increased from $\Lambda \approx 1$ to $\Lambda \approx 4$.

Opposite to a configuration with a large density contrast where the structure of the convection pattern consists of isolated, broad warm upflows and narrow network-like, cold and strong downflows, within a weakly stratified layer the separation of up- and downflows is less pronounced. Instead the upflows form a kind of unconnected single plume-like structures enclosed by a loosely connected broad network of downflows. Up- and downflows are of approximately

equal amplitude and occupy roughly an equal area in the horizontal plane.

To characterize the anisotropy of the turbulence and to quantify the visual impression obtained from Fig. 2 the average extension of a convection cell is estimated in both horizontal directions. The two-point correlation function Q_{zz} is defined for the direction perpendicular to the imposed magnetic field by

$$Q_{zz}(\delta x) = \frac{\langle u'_z(x)u'_z(x + \delta x) \rangle}{\langle u'_z(x)^2 \rangle} \quad (12)$$

and for the direction parallel to the field:

$$Q_{zz}(\delta y) = \frac{\langle u'_z(y)u'_z(y + \delta y) \rangle}{\langle u'_z(y)^2 \rangle}. \quad (13)$$

Q_{zz} can be used as a convenient measure for the average horizontal extension of a convection cell. Motions within a cell are oriented in the same direction so that they are highly correlated whereas no correlations exist if the distance between the considered two points (given by δx , respectively δy) exceeds the size of the cell. The mean cell size is interpreted as the correlation length λ_{corr} or Taylor microscale, which is the characteristic length-scale of the vorticity filaments observed in swirling flows. λ_{corr} is estimated from a function f , defined as

$$f(\delta x) = 1 - \lambda_{\text{corr}}^{-2}(\delta x)^2 \quad (14)$$

which is adjusted to the decreasing part of the two-point correlation function Q_{zz} .

Figure 3 shows $Q_{zz}(\delta x)$ (upper panel) and $Q_{zz}(\delta y)$ (lower panel) for $\Lambda = 0.1, 1, 10, 100$ (solid curves) and the corresponding functions f (dashed curves). The shape of the curves of Q_{zz} resembles the decrease of the correlation of the turbulent vertical velocity at two different coordinates with increasing distance between these two points. The behavior of $Q_{zz}(\delta x)$ which determines the correlation length perpendicular to B_y is independent of the imposed field strength (therefore the curves in the upper panel of Fig. 3 are not labeled by Λ). However, for large δx the curves in the upper panel exhibit an oscillating-like structure, which evolves in dependence of the field strength. With increasing field strength the amplitude increases and the length scale of these oscillations decreases. In case of weak fields the correlations outside of one cell are averaged out due to the disordered occurrence of convection cells. For strong fields the sheetlike structures that can be observed on the lower right panel of Fig. 2 establish a more ordered structure which resembles in the oscillations of the correlation function in the upper panel of Fig. 3.

The influence of the magnetic field on the cell structure is considerably pronounced in the lower panel of Fig. 3 where Q_{zz} is broadened with increasing field strength. The resulting correlation lengths $\lambda_{x,y}^{\text{corr}}$ – estimated independently for both horizontal directions from Eq. (14) – are shown in Fig. 4. The black curve denotes the case $\text{Ta} = 10^6$ where the solid (dotted) line represents λ_x^{corr} (λ_y^{corr}). The gray curve shows the same quantities for $\text{Ta} = 10^7$. As already indicated in the upper panel of Fig. 3, for both rotation rates, λ_x^{corr} is nearly independent from the field strength so that the extension of the cell in x -direction is only determined by the rotation rate. According to the linear theory the preferred length scale for the onset of rotating convection scales

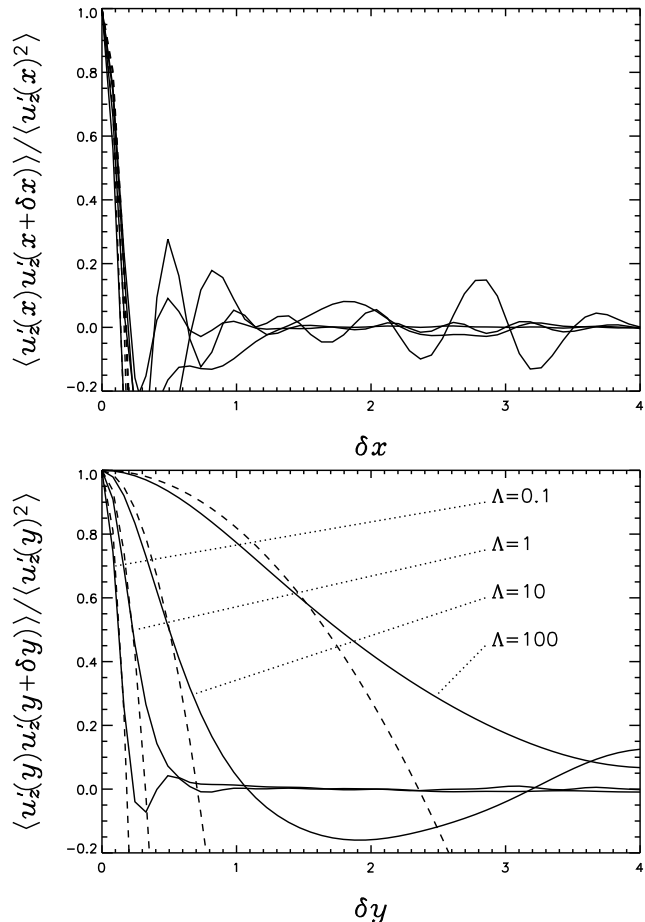


Figure 3. Time average of the two-point-correlation functions. The solid lines represent $Q_{zz}(\delta x)$, respectively $Q_{zz}(\delta y)$ and the dashed lines represent a fit according to Eq. (14) to the innermost part of Q_{zz} . $\text{Ta} = 10^7$, $\theta = 0^\circ$, $\Lambda \approx 0.1, 1, 10, 100$.

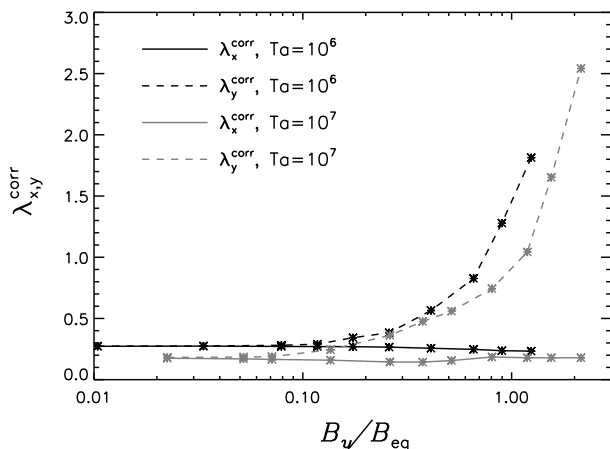


Figure 4. Time and volume average of the correlation length $\lambda_{x,y}^{\text{corr}}$ in x - and y -direction in dependence of the imposed magnetic field strength. The solid (dotted) line denotes the extension in x -direction (y -direction) for $\text{Ta} = 10^6$ (black) and for $\text{Ta} = 10^7$ (gray). $\theta = 0^\circ$.

as $Ta^{-1/6}$ (for sufficient fast rotation). Scaling laws for rotating finite amplitude convection have been examined by Stellmach & Hansen (2004). They confirmed the above denoted scaling law for the size of a convection cell by evaluating the preferred wave number $k = 1/\lambda^{\text{corr}}$ from the maximum value of the kinetic energy spectra. Within the rather restricted range of rotation rates our results reconfirm this scaling for λ_x^{corr} :

$$\frac{\lambda_x^{\text{corr}}(Ta = 10^6)}{\lambda_x^{\text{corr}}(Ta = 10^7)} \approx 1.5 \approx \left(\frac{10^6}{10^7}\right)^{-\frac{1}{6}}.$$

The correlation length parallel to the imposed field, λ_y^{corr} , resembles the increasing extension of the convection cells in direction of the imposed field. The field strength at which the transition to an anisotropic, elongated cell occurs only weakly depends on the rotation rate, however, the increase of λ_y^{corr} is slightly stronger for slower rotation.

For increasing co-latitude θ the convection cells become more and more tilted (according to the Taylor-Proudman theorem). For a higher co-latitude, λ_x^{corr} increases due to this geometric effect, whereas λ_y^{corr} remains nearly unaffected (corresponding plots are omitted).

The anisotropic character of the turbulence is also apparent in the behavior of the turbulence intensities $\langle u_i'^2 \rangle$. For a quantitative examination the following functions are introduced:

$$A_H = \frac{\langle u_y'^2 \rangle - \langle u_x'^2 \rangle}{u_{\text{rms}}^2} \quad A_V = \frac{\langle u_x'^2 \rangle + \langle u_y'^2 \rangle - 2\langle u_z'^2 \rangle}{u_{\text{rms}}^2} \quad (15)$$

(see also Käpylä et al., 2004, and note the different definition for A_V). The anisotropy of the turbulence intensities is described by A_H and A_V in the following way:

$$A_H \begin{cases} < 0 & \text{dominated by turbulence perpendicular to } B_{\text{al}} \\ = 0 & \text{horizontal isotropy} \\ > 0 & \text{dominated by turbulence parallel to } B_y \end{cases}$$

$$A_V \begin{cases} < 0 & \text{dominated by vertical turbulence} \\ > 0 & \text{dominated by horizontal turbulence} \end{cases}$$

As expected, in the presence of a magnetic field the motions perpendicular B_y are more strongly suppressed than the motions parallel B_y . The resulting behavior of A_H at $\theta = 0^\circ$ is shown in the upper panel of Fig. 5 which denotes the transition from the horizontal isotropic turbulence to an anisotropic state. A dependence on the rotation rate is evident. For $Ta = 10^6$ we approximately obtain horizontal isotropy up to field strengths corresponding to $B \approx 0.4B_{\text{eq}}$ ($\Lambda \approx 10$) whereas faster rotation results in $A_H > 0$ except for very weak magnetic fields.

The vertical anisotropy, A_V , is presented in the lower panel of Fig. 5. For negligible magnetic fields an increase of the rotation velocity leads to an isotropic behavior on the small scales ($A_V \rightarrow 0$ for $B \rightarrow 0$), a property that has been found by Brummell et al. (1996). Already weak horizontal fields break this tendency and result in a turbulence which is dominated by the vertical component. Independent from the rotation rate the vertical anisotropy exhibits a maximum around $B_y \approx 0.3B_{\text{eq}}$. The dominance of the vertical component is characteristic for the behavior of the turbulence close to the pole and is not maintained for higher co-latitudes. The transition from vertical to horizontal dominated turbulence is determined by the orientation of the coherent cell struc-

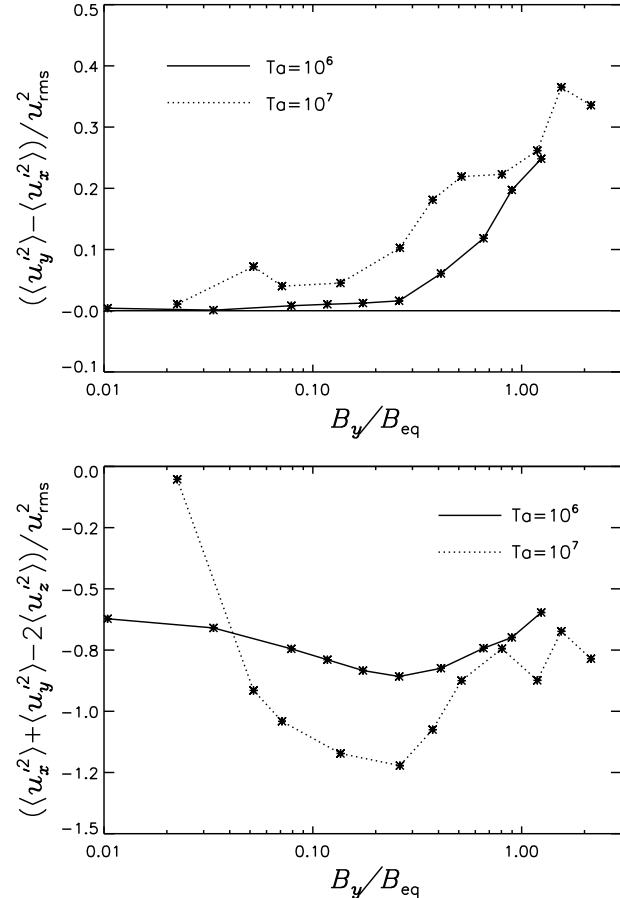


Figure 5. Upper panel: Time and volume average of the horizontal anisotropy A_H for $Ta = 10^6$ (solid line) and $Ta = 10^7$ (dotted line). Lower Panel: Time and volume average of the vertical anisotropy A_V for $Ta = 10^6$ (solid line) and $Ta = 10^7$ (dotted line). $\theta = 0^\circ$.

tures, i.e. by the orientation along the rotation axis and by the elongation parallel to the dominant field component.

3.2 Turbulent heat flux

3.2.1 General description of the turbulent transport of heat

For statistically steady convection the turbulent heat flux F_i^{conv} is given by:

$$F_i^{\text{conv}} = \rho c_p \langle u_i' T' \rangle = \kappa_{ij} \left(\frac{\partial T}{\partial x_j} - \frac{g_j}{c_p} \right) \quad (16)$$

(see e.g. Rüdiger, 1989) where κ_{ij} denotes the tensorial heat conductivity which is related to the thermal diffusivity tensor χ_{ij} by $\kappa_{ij} = \rho c_p \chi_{ij}$. In the presented model the large-scale temperature gradient $\partial T / \partial x_j$ and the gravity g are constant and oriented parallel to the z -axis so that we are only able to discuss the case $j = z$. Since, in addition, the density ρ remains approximately constant within the computational domain the simple relation $\kappa_{iz} \propto \langle u_i' T' \rangle$ holds to a good approximation and, in principal, κ_{iz} can immediately be determined from the numerically computed correlations $\langle u_i' T' \rangle$. It is convenient to define a normalized heat flux

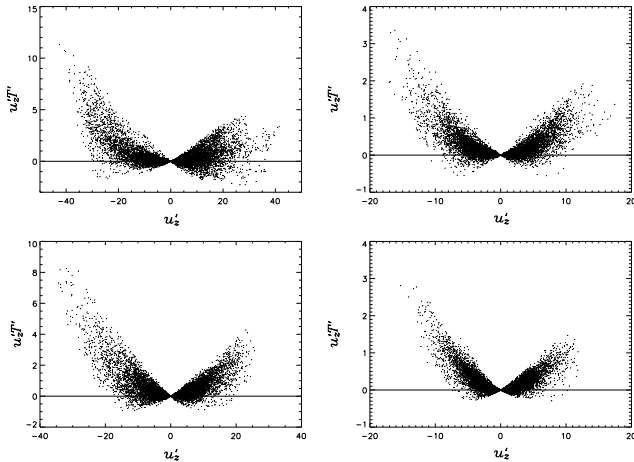


Figure 6. Scatter plot of the normalized vertical heat flux in dependence of the turbulent up- and downflows at $z = 0.5$. Upper left panel: convection, upper right panel: rotating convection ($Ta = 10^7$, $\theta = 45^\circ$), lower left panel: magnetoconvection ($B_z \approx 0.2B_{\text{eq}}$), lower right panel: rotating magnetoconvection, $\Lambda = 1$ (corresponds to $B_y \approx 0.2B_{\text{eq}}$, $Ta = 10^7$ and $\theta = 45^\circ$).

$$\widehat{F}_i^{\text{conv}} = \frac{F_i^{\text{conv}}}{\rho c_p} = \langle u'_z T' \rangle = \chi_{iz} \left(\frac{\partial T}{\partial z} - \frac{g_z}{c_p} \right) \quad (17)$$

which is the quantity that is discussed with regard to the turbulent transport of heat in the remainder of this paper.

The vertical heat flux is caused by turbulent upflows of warmer fluid and downflows of cooler fluid. Mainly the fastest up- and downflows contribute to the net flux which can be seen in Fig. 6 where time snapshots of the normalized flux $u'_z T'$ evaluated in a horizontal plane at $z = 0.5$ are presented in various scatter plots. Each dot denotes $u'_z T'$ at a certain grid cell in dependence of the local vertical velocity u'_z . The sum of all values (divided by the number of data points) represents the horizontal average of $\langle u'_z T' \rangle$ at $z = 0.5$. The four panels show the results from simulations of convection (upper left panel), rotating convection (upper right panel), magnetoconvection (lower left panel) and rotating magnetoconvection (lower right panel). Qualitatively the behavior is similar for all four rather different states which only distinguish in the amplitude of $u'_z T'$ and of the velocity u'_z . The downflows ($u'_z < 0$) and the upflows ($u'_z > 0$) contribute with nearly the same amount to the net flux (although it seems that the downflows are slightly prevailing). This differs from the results for a strongly stratified layer presented by Ziegler (2002) who obtained a preponderance of the contributions by the downflows in non-rotating magnetoconvection which does not occur in sufficient fast rotating magnetoconvection.

Typical volume averaged values of the vertical heat flux for moderate field strength and $Ta = 10^7$ are given by $\langle u'_z T' \rangle \approx 0.2$ (in code units, see also section 3.2.2.). From Eq. (17) we therefore retrieve $\chi_{zz} \approx 0.4$, which is about four times larger than the value for the molecular diffusivity $\chi = 0.1$ as it results from the input parameters (all numbers in code units, see section 2.3 and 2.5). Although only moderate turbulence is examined, the obtained coefficient for the vertical transport of heat exceeds the molecular one, so that

the transport of heat by turbulent motions is more effective than the molecular transport through heat conduction.

3.2.2 Vertical heat flux and turbulence intensity

From the quasi-linear theory a simple expression relating the thermal diffusivity tensor χ and \widehat{Q}_{ij} , the Fourier transform of the one-point correlation tensor $\widetilde{Q}_{ij} = \langle u'_i(\mathbf{x}, t) u'_j(\mathbf{x}, t) \rangle$ exists:

$$\chi_{ij} = \int \int \frac{\chi k^2 \widehat{\widetilde{Q}}_{ij}(\mathbf{k}, \omega)}{\omega^2 + \chi^2 k^4} d\mathbf{k} d\omega. \quad (18)$$

For $\chi \rightarrow 0$, the integrand can be replaced by a δ -function, so that:

$$\chi_{ij} = \pi \int \widehat{\widetilde{Q}}_{ij}(k, 0) dk = \frac{1}{2} \int \widetilde{Q}_{ij}(0, \tau) d\tau \approx \frac{1}{2} \tau_{\text{corr}} \widetilde{Q}_{ij} \quad (19)$$

where the τ -integral is approximated by τ_{corr} , the correlation time of the turbulence. A detailed explanation can be found in Rüdiger (1989). This is a rather rough estimation which is based on the possibility to express the temperature fluctuations T' through the fluctuating velocity u' and is valid in the mixing-length approximation, where the turbulence spectra is dominated by one scale: $\sim \delta(k - \tau_{\text{corr}}^{-1}) \delta(\omega)$. Eq. (19) might not be appropriate for a fast rotating system under the simultaneous influence of a magnetic field but it should deliver a general tendency for a relation between the turbulent velocity fluctuations and the (turbulent) thermal diffusivity tensor, respectively the normalized heat flux $\widehat{F}_i^{\text{conf}}$.

In Fig. 7 the behavior of the vertical turbulence intensity $\langle u_z'^2 \rangle$ (upper panel) is compared with the development of the normalized vertical heat flux, $\langle u'_z T' \rangle$ (lower panel) for $Ta = 10^7$. Here, only the differences between the pole (solid line) and a co-latitude at $\theta = 45^\circ$ (dotted line) are pointed out. A more detailed analysis of the angular dependence is given in the next section (3.2.4). As the most characteristic feature $\langle u_z'^2 \rangle$ increases with increasing field strength and exhibits a sharp drop for $\Lambda \gtrsim 2$ at $\theta = 0^\circ$. The maximum value for $\langle u_z'^2 \rangle$ is retrieved around $\Lambda \approx 1 \dots 2$. In this parameter regime (where Lorentz force and Coriolis force are of the same order of magnitude) the turbulence is enhanced compared to rotating non-magnetic convection. This feature does not appear at $\theta = 45^\circ$ or for a slower rotation rate (Fig. 8). The enhanced turbulence around $\Lambda \approx 1$ has been predicted by Chandrasekhar (1961) who showed that the critical Rayleigh number Ra_{crit} is minimal if Lorentz and Coriolis forces are comparable. In case of a fixed (overcritical) Rayleigh number a drop of Ra_{crit} leads to a more overcritical convection which results in a stronger driven flow and a more vigorous turbulence occurs. Although the linear stability analysis of Chandrasekhar (1961) has been performed for a vertical oriented field (B_z), the general trend might also be true for a horizontal field. From the linear analysis it is also known that this effect is more pronounced for faster rotating systems so that the maximum structure of $\langle u_z'^2 \rangle$ will be more dominant for even faster rotation, a result that already has been confirmed by Stellmach & Hansen (2004). However, the authors also obtained hints, that this effect – predicted from a linear stability analysis – vanishes

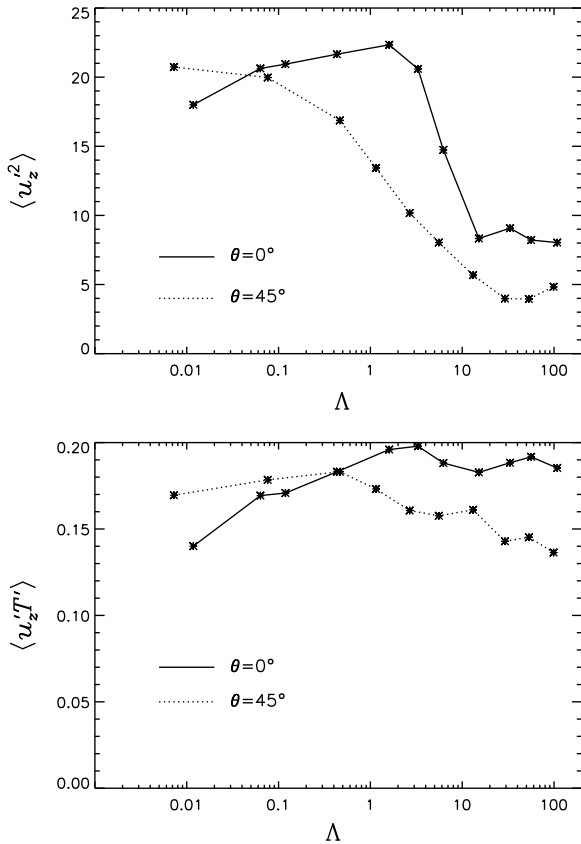


Figure 7. Time and volume average of the turbulence intensity and heat flux in dependence of the Elsässer number Λ . Upper panel: $\langle u_z'^2 \rangle$, lower panel: $\langle u_z'T' \rangle$. $Ta = 10^7$.

for stronger driven flows where the non-linearities dominate the final state.

In accordance with the behavior of $\langle u_z'^2 \rangle$ the normalized vertical heat flux increases with the field strength below $\Lambda \approx 1$, but $\langle u_z'T' \rangle$ remains at a high level and only weakly decreases for strong fields. Although the fluctuating fluid motions are inhibited in the presence of a strong magnetic field, this is obviously not the case for the temperature fluctuations, so that the correlation of these two quantities is not suppressed with increasing field strength. This feature is not observable at a higher co-latitude where $\langle u_z'T' \rangle$ exhibits a maximum around $\Lambda \approx 0.5$.

A second distinctive feature is reflected in the crossover of the two curves for $\theta = 0^\circ$ and $\theta = 45^\circ$ in Fig. 7. For weak fields the turbulence intensity and the vertical heat flux at $\theta = 45^\circ$ are larger than at the pole whereas both quantities behave the other way round for a field strength above $\Lambda \approx 0.1 \dots 0.5$. Such a behavior does not occur for slower rotation (see Fig. 8) or in case of a vertically oriented field (Fig. 9). The vertical turbulence intensity and heat flux under influence of an external imposed B_z are illustrated in Fig. 9 (note, that in this case the magnetic boundary conditions have to be changed to $B_x = B_y = 0$ and $\partial_z B_z = 0$). Independent of the field strength, $\langle u_z'^2 \rangle$ and $\langle u_z'T' \rangle$ are slightly larger at 45° and both quantities show nearly the same dependence on the field strength. At the pole both

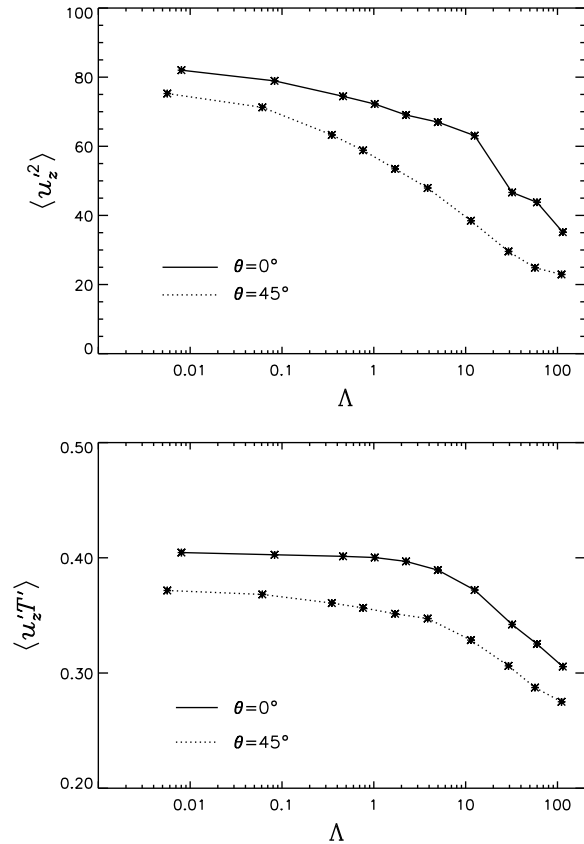


Figure 8. Time and volume average of the turbulence intensity $\langle u_z'^2 \rangle$ and the turbulent heat flux $\langle u_z'T' \rangle$ for $Ta = 10^6$.

quantities exhibit a weakly pronounced maximum around $\Lambda \approx 1$ and a very effective suppression occurs for $\Lambda \gtrsim 2$.

3.2.3 Horizontal heat fluxes and Reynolds stresses

In the following, again, a horizontal field is imposed and the horizontal transport of heat is discussed. The horizontal components of the normalized heat flux, $\langle u_x'T' \rangle$ and $\langle u_y'T' \rangle$ and the corresponding Reynolds stresses \tilde{Q}_{xz} and \tilde{Q}_{yz} vanish at the poles. This expected behavior is nearly perfectly reflected in the numerical results and therefore the dependence on the field strength is only considered at $\theta = 45^\circ$. Figure 10 shows \tilde{Q}_{xz} and \tilde{Q}_{yz} (upper panel) in comparison with $\langle u_x'T' \rangle$ and $\langle u_y'T' \rangle$ (lower panel). In all cases the considered quantities are negative. Therefore, the latitudinal component, $\langle u_x'T' \rangle$, describes a transport of heat towards the (north-)pole. The absolute value increases with increasing field strength whereas the absolute value of \tilde{Q}_{xz} decreases with increasing field strength. As a consequence the relation between $\langle u_x'T' \rangle$ and \tilde{Q}_{xz} cannot be described by a simple expression given by Eq. (19).

In a spherical geometry the y -component of the heat flux corresponds to an azimuthal transport of heat. $\langle u_y'T' \rangle$, as it is also always negative, describes a westward directed transport of heat. The absolute value exhibits a distinct maximum value around $\Lambda \approx 10$ and for very strong fields $\langle u_y'T' \rangle$ vanishes. The behavior of the azimuthal heat flux

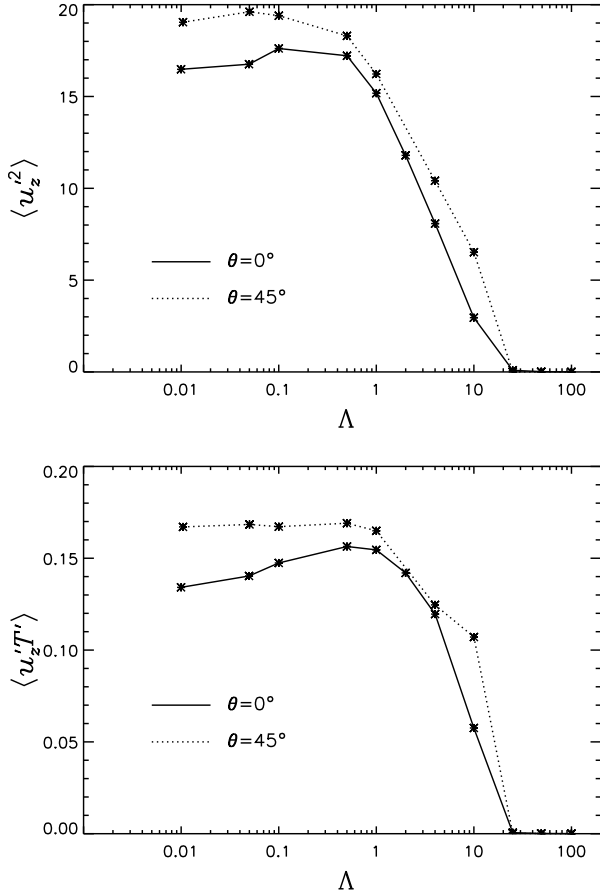


Figure 9. Time and volume average of vertical turbulence intensity (upper panel) and vertical heat flux (lower panel) in case of a vertical oriented magnetic field (B_z). $Ta = 10^7$.

roughly resembles the profile of \tilde{Q}_{yz} , although there exists a small offset for the location of the minimum of \tilde{Q}_{yz} towards weaker magnetic fields.

3.2.4 Angular dependence

In case of rotating turbulence without any other preferred direction the turbulent diffusivity tensor χ_{ij} is given by

$$\chi_{ij} = \chi_T \delta_{ij} + \chi_{||} \frac{\Omega_i \Omega_j}{\Omega^2} + \tilde{\chi} \epsilon_{ipj} \Omega_p \quad (20)$$

(see e.g. Kitchatinov et al. 1994). $\chi_{||}$ describes enhanced thermal diffusion parallel to the rotation axis and the expression $\tilde{\chi} \epsilon_{ipj} \Omega_p$ describes enhanced/reduced diffusion in the azimuthal direction (which can be neglected in an axisymmetric configuration). In the applied Cartesian system where we are restricted to a vertical large scale temperature gradient the following three elements of χ_{ij} can be computed:

$$\chi_{xz} = -\chi_{||} \sin \theta \cos \theta \quad (21)$$

$$\chi_{yz} = -\tilde{\chi} \Omega \sin \theta \quad (22)$$

$$\chi_{zz} = \chi_T + \chi_{||} \cos^2 \theta \quad (23)$$

These expressions neglect the influence of the magnetic field and might therefore be valid only for small values of Λ .

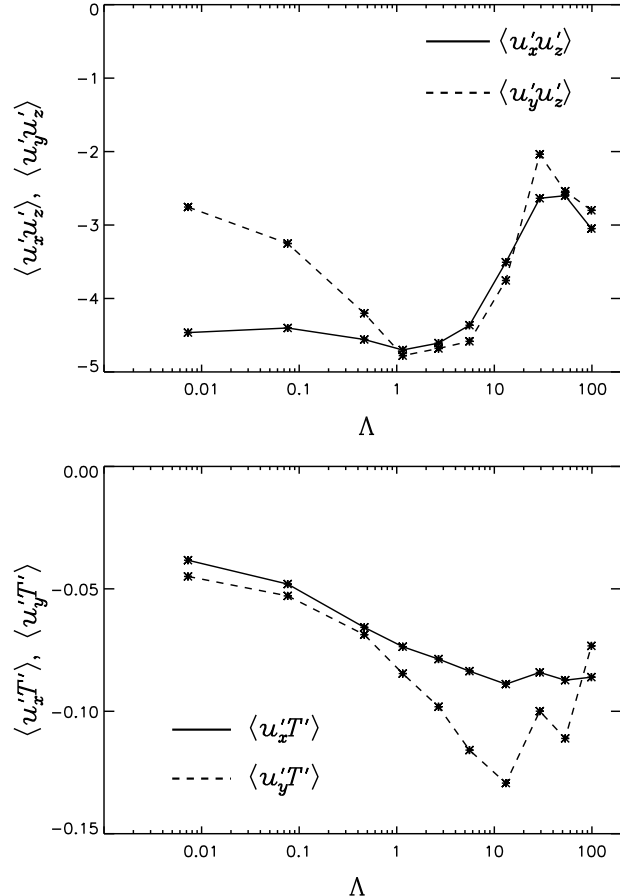


Figure 10. Time and volume average of horizontal Reynolds stresses $\langle u_x' u_z' \rangle$ (upper panel) and normalized heat flux $\langle u_{x,y}' T' \rangle$ (lower panel) in dependence of the imposed magnetic field strength. $\theta = 45^\circ$ and $Ta = 10^7$.

The angular dependence of the Reynolds stresses and the normalized turbulent heat flux are shown in Fig. 11 (left hand side: \tilde{Q}_{iz} ; right hand side $\langle u_i' T' \rangle$). The solid (dotted, dashed) lines denote the results for $\Lambda = 0.1(1, 10)$ (corresponding to $B_y = 0.07(0.2, 0.7)B_{eq}$). In all cases the meridional component $\langle u_x' T' \rangle$ is negative. For $\Lambda \approx 0.1$ and $\Lambda \approx 1$ the absolute value exhibits a maximum around $\theta = 45^\circ$ and in both cases $\langle u_x' T' \rangle$ can be described by a function $\propto \sin \theta \cos \theta$ as indicated by equation (21).

The azimuthal component $\langle u_y' T' \rangle$ is also always negative and the absolute values increase towards the equator so that at least the tendency coincides with the behavior indicated by expression (22). $|\langle u_y' T' \rangle|$ increases with increasing B_y which becomes more pronounced towards the equator.

The vertical component $\langle u_z' T' \rangle$ is always positive thus heat is transported outwards. For $\Lambda \lesssim 1$ the vertical heat flux increases towards the equator and, in principle, the behavior could be approximated by an expression of the form given by equation (23). This is only possible if $\chi_{||}$ is negative. However, a negative value for $\chi_{||}$ is in contradiction with the results for the meridional heat flux which require $\chi_{||} > 0$. A positive value for $\chi_{||}$ is also obtained from calculations of Kitchatinov et al. (1994). Regarding the Coriolis force at the pole, $\boldsymbol{\Omega} \times \mathbf{u} = \Omega_0(-u_y, u_x, 0)$, it is evident that no (lin-

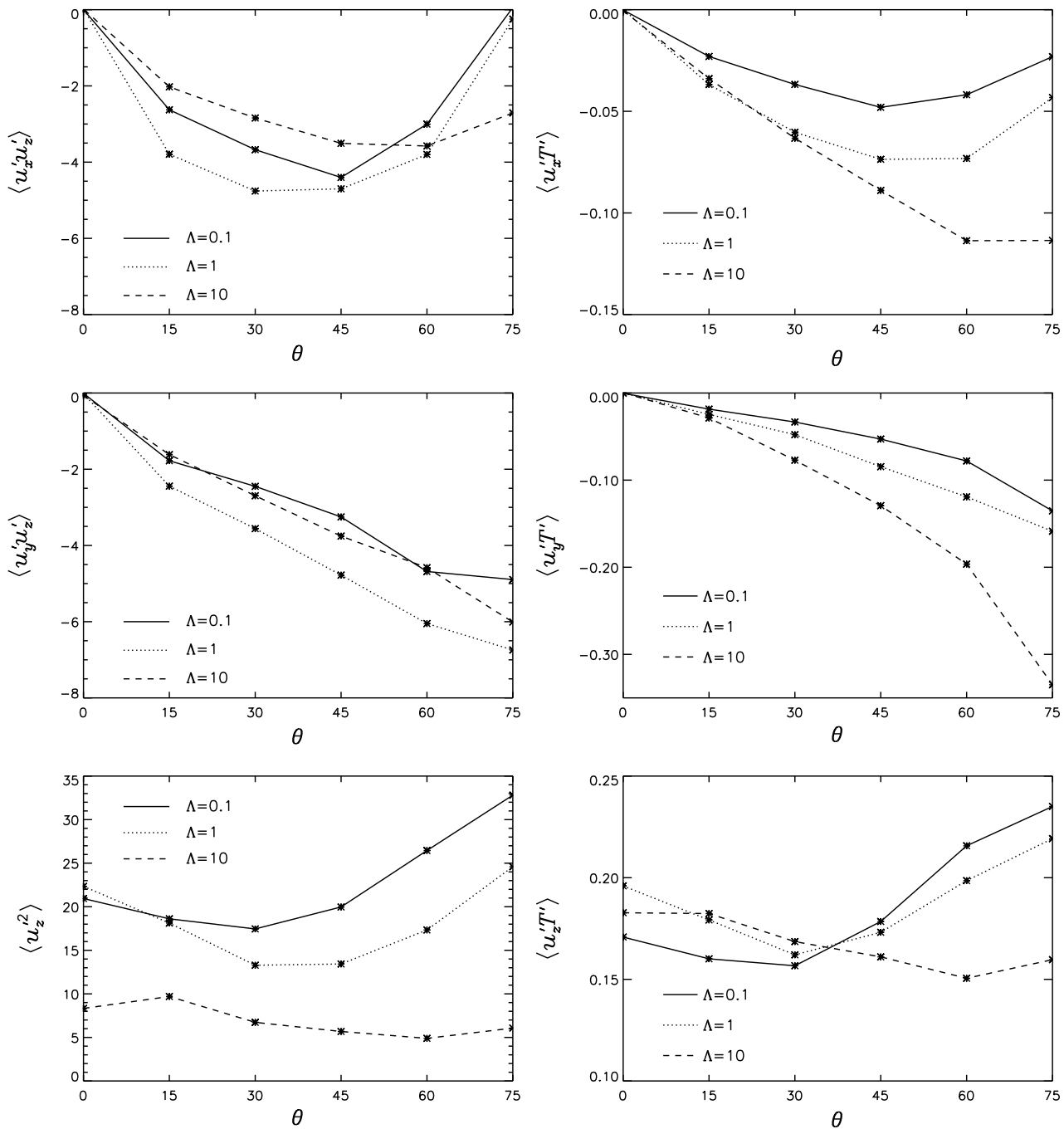


Figure 11. Left side: Time and volume averages of the Reynolds stresses \tilde{Q}_{xz} , \tilde{Q}_{yz} and \tilde{Q}_{zz} . Right side: Time and volume averages of the heat fluxes $\langle u'_x T' \rangle$, $\langle u'_y T' \rangle$ and $\langle u'_z T' \rangle$. Both quantities are shown in dependence of the co-latitude θ for $Ta = 10^7$. The solid (dotted, dashed) curve denotes $\Lambda = 0.1(1, 10)$.

ear) coupling between vertical and horizontal components is possible. A transfer of vertical and horizontal momentum (through the coupling of u_z with u_x respectively u_y) is only possible at higher co-latitude. Therefore one could suppose that quantities, like the vertical heat flux or the vertical component of the turbulence intensity are maximum at the pole and decrease towards the equator. The somehow surprising opposite behavior shown in the simulations here, is confirmed the numerical results of Käpylä et al. (2004) and

Rüdiger et al. (2005). Käpylä et al. (2004) calculated the vertical and the meridional heat flux for rotating convection in a strongly stratified layer for a various number of rotation rates. In all cases they report the maximum of the vertical heat flux at the equator and “a tendency” for the minimum at a co-latitude $\theta \approx 30^\circ \dots 45^\circ$. These results are confirmed by our calculations up to $\Lambda \approx 1$. Only for strong magnetic fields ($\Lambda \approx 10$) the vertical turbulence intensity and heat flux are larger at the pole.

4 DISCUSSION AND CONCLUSIONS

Rotating magnetoconvection has been examined for a wide range of parameters and due to the varieties of the results it is nearly impossible to describe the outcome uniformly. The convectively driven flow changes its characteristic properties considerably in dependence of the applied magnetic field and/or rotation rate. The behavior of the cell pattern indicates that in case of a dominant toroidal field convection in a fast rotating system should occur in extremely thin sheet like structures. In the presented simulations the vertical extension of the cells is fixed by the vertical boundary conditions so that the average size of the convection cells in z -direction is extended over the whole box domain. It is hardly believable that such structures are stable over the largest possible scales given by the size of the fluid outer core so that the “real” vertical structure of the convection remains dubious and might only be obtained from, at present unrealistic, global high-resolution simulations.

For faster rotation the effects of the magnetic field on the fluid flow via the Lorentz force become more significant. This has been shown by the behavior of the anisotropy functions A_H and A_V . Particular attention deserves the vertical anisotropy. The isotropic behavior on the small scales caused by rotation vanishes with the introduction of a magnetic field. As a consequence, the vertical component of the turbulence intensity dominates the flow which leads to an enhanced vertical mixing of the convective layer. Turbulent transport in a rotating system is facilitated through the introduction of a magnetic field.

The turbulent heat flux has been calculated as an example for a diffusive process that occurs on scales that are not resolved in global simulations. Most remarkably, the vertical heat flux at the pole slightly increases with increasing magnetic field strength (if the rotation is fast enough) and remains at a high level even for very strong magnetic fields. Thus, cooling of the Earth’s interior is enhanced by the presence of a dominant toroidal field. Comparison of the results from non-rotating magnetoconvection with simulations that involve rotation and a horizontal (Fig. 7) or a vertically oriented magnetic field (Fig. 9), respectively, shows that an enhancement of the vertical heat flux at high field strength only occurs in combination of a horizontally oriented magnetic field, a sufficient fast rotation rate and close to the north-pole. However, the effects of B_y on the vertical heat transport are relatively small compared to the strong quenching for $\Lambda \gtrsim 2 (B \gtrsim 0.3 B_{\text{eq}})$ in case of an imposed B_z .

Likewise of interest is the behavior of the meridional heat flux which is always negative, indicating that heat is transported towards the poles. From comparison with slower rotating magnetoconvection we know that the rotational quenching of $\langle u_x T' \rangle$ is weaker than for $\langle u_y T' \rangle$ and $\langle u_z T' \rangle$, so that it might be possible that in a fast rotating system a significant amount of heat is transported towards the poles. Therefore, the poles should be warmer than the equator. This results in a non-radial oriented large-scale temperature gradient which acts as a source for a meridional large-scale flow. Such a meridional flow – if strong enough – interacts with the column like large-scale structure of the convective motions and might be important for the understanding of the dynamo mechanism in the Earth’s core (see e.g. Sarson & Jones (1999), who identified a fluctuating meridional flow

as an explanation for the occurrence of dipole reversals). Indeed, global simulations of Olson & Christensen (2002) yield a warmer northpole (see their Fig. 5) but it is not clear if this effect is a result of turbulent heat transport. A large scale meridional flow is also found in the solar convection zone, giving rise to important consequences for the solar rotation law (Rüdiger et al., 2005).

The distribution of the temperature on the top of the fluid core depends on the heat flow at the core mantle boundary that is usually prescribed as a boundary condition. Seismological measurements indicate a non-uniform heat flow at the core mantle boundary, whose influence has been examined in numerical simulations of Olson & Christensen (2002). The lateral and longitudinal variations of the boundary heat flux affect the local behavior of the fluid flow: convection is enhanced (inhibited) where the boundary heat flow is high (low). In case of non-axisymmetric boundary conditions at the top of the fluid core, the azimuthal heat flux becomes important. The azimuthal heat flux is always negative and increases towards the equator. This leads to a latitude dependent westward transport of heat which should interact with the constraints given by the inhomogeneous thermal conditions at the core mantle boundary.

Most considerations within the presented work rely on the assumption of a dominant toroidal field within the fluid core. This does not have to be necessarily the case. Due to the insulating mantle the toroidal component of the Earth’s magnetic field is hidden from any observations. Indeed, most of the authors favor a geodynamo-model of $\alpha\Omega$ -type (Fearn 1998) which is characterized by a dominant azimuthal field. However, estimations of the toroidal field strength from the extrapolation of the dc electric potential near the top of the Earth’s mantle to the core mantle boundary result in comparable strength of the toroidal and the poloidal field components (Levy & Pearce, 1991). Furthermore, recent simulations of Christensen & Aubert (2006) that cover a very large parameter space, yield solutions without significant differential rotation where poloidal and toroidal field strength are comparable (α^2 -Dynamo).

Independent from the orientation of the dominant field component, the direction of the horizontal components of the heat flux (towards the poles and westwards, i.e. against the direction of the rotation) is a consequence of the rotation and not caused by the magnetic field which only enhances or reduces the magnitude of the heat flux. Therefore the horizontal components of the heat flux should show a similar sign even in case of comparable toroidal and poloidal field strength.

The circumstances within a rotating spherical shell are more complicated as they appear in the presented Cartesian model where relevant characteristics have not been concerned for simplicity. In particular, the combined effects of all three components of the turbulent heat flux cannot be inferred from a simple local model so that the consequences of the common behavior could only be examined by a global simulation. However, the results should at least qualitatively resemble the combined effects of the small scale fluctuations on large scale fields and comparable effects are expected to be present in spherical geometries. To what extend the reported results for the heat flux will endure in simulations in spherical geometry, where also possible larger scale flows will

occur, again can only be clarified in highly resolved global simulations.

REFERENCES

- Braginsky, S. I. & Meytlis, V. P., 1990. Local turbulence in the earth's core, *Geophysical and Astrophysical Fluid Dynamics*, **55**, 71–87.
- Brummell, N. H., Hurlburt, N. E., & Toomre, J., 1996. Turbulent Compressible Convection with Rotation. I. Flow Structure and Evolution, *Astrophysical Journal*, **473**, 494.
- Buffett, B. A., 2003. A comparison of subgrid-scale models for large-eddy simulations of convection in the Earth's core, *Geophysical Journal International*, **153**, 753–765.
- Bushby, P. J., 2003. Modelling dynamos in rapidly rotating late-type stars, *Mon. Not. R. astr. Soc.*, **342**, L15–L19.
- Cattaneo, F., Emonet, T., & Weiss, N., 2003. On the Interaction between Convection and Magnetic Fields, *Astrophysical Journal*, **588**, 1183–1198.
- Chandrasekhar, S., 1961. *Hydrodynamic and hydromagnetic stability*, International Series of Monographs on Physics, Oxford: Clarendon.
- Christensen, U. R. & Aubert, J., 2006. Scaling properties of convection-driven dynamos in rotating spherical shells and application to planetary magnetic fields, *Geophys. J. Int.*, **166**, 97–114.
- Eschrich, K.-O. & Krause, F., 1977. Anisotropic heat transport as a possible explanation for the temperature distribution in sunspots, *Astronomische Nachrichten*, **298**, 1–8.
- Fearn, D. R., 1998. Hydromagnetic flow in planetary cores, *Reports of Progress in Physics*, **61**, 175–235.
- Giesecke, A., Ziegler, U., & Rüdiger, G., 2005. Geodynamo α -effect derived from box simulations of rotating magnetoconvection, *Phys. Earth planet. Inter.*, **152**, 90–102.
- Hollerbach, R., 2003. The range of timescales on which the geodynamo operates, *Geodynamics Series*, **31**, 181–192.
- Jackson, A., 2003. Intense equatorial flux spots on the surface of Earth's core, *Nature*, **424**, 760–763.
- Käpylä, P. J., Korpi, M. J., & Tuominen, I., 2004. Local models of stellar convection: Reynolds stresses and turbulent heat transport, *Astronomy and Astrophysics*, **422**, 793–816.
- Kitchatinov, L. L., Pipin, V. V., & Rüdiger, G., 1994. Turbulent viscosity, magnetic diffusivity, and heat conductivity under the influence of rotation and magnetic field, *Astronomische Nachrichten*, **315**, 157–170.
- Levy, E. H. & Pearce, S. J., 1991. Steady state toroidal magnetic field at earth's core-mantle boundary, *J. geophys. Res.*, **96**, 3935–3942.
- Matsui, H. & Buffett, B. A., 2005. Sub-grid scale model for convection-driven dynamos in a rotating plane layer, *Phys. Earth planet. Inter.*, **153**, 108–123.
- Matsushima, M., 2004. Scale similarity of MHD turbulence in the Earth's core, *Earth, Planets, and Space*, **56**, 599–605.
- Matsushima, M., 2005. A scale-similarity model for the subgrid-scale flux with application to MHD turbulence in the Earth's core, *Phys. Earth planet. Inter.*, **153**, 74–82.
- Matsushima, M., Nakajima, T., & Roberts, P. H., 1999. The anisotropy of local turbulence in the Earth's core, *Earth Planets Space*, **51**, 277–286.
- Olson, P. & Christensen, U. R., 2002. The time-averaged magnetic field in numerical dynamos with non-uniform boundary heat flow, *Geophysical Journal International*, **151**, 809–823.
- Phillips, C. G. & Ivers, D. J., 2001. Spectral interactions of rapidly-rotating anisotropic turbulent viscous and thermal diffusion in the Earth's core, *Phys. Earth planet. Inter.*, **128**, 93–107.
- Phillips, C. G. & Ivers, D. J., 2003. Strong field anisotropic diffusion models for the Earth's core, *Phys. Earth planet. Inter.*, **140**, 13–28.
- Roberts, P. H. & Glatzmaier, G. A., 2000. Geodynamo theory and simulations, *Reviews of Modern Physics*, **72**, 1081–1123.
- Rüdiger, G., 1989. *Differential rotation and stellar convection. Sun and the solar stars*, Berlin: Akademie Verlag, 1989.
- Rüdiger, G. & Hollerbach, R., 2004. *The Magnetic Universe - Geophysical and Astrophysical Dynamo Theory*, Wiley-VCH Verlag Berlin.
- Rüdiger, G. & Kitchatinov, L. L., 2000. Sunspot decay as a test of the eta-quenching concept, *Astronomische Nachrichten*, **321**, 75–80.
- Rüdiger, G., Egorov, P., Kitchatinov, L. L., & Küker, M., 2005. The eddy heat-flux in rotating turbulent convection, *Astronomy and Astrophysics*, **431**, S. 345–352.
- Sarson, G. R. & Jones, C. A., 1999. A convection driven geodynamo reversal model, *Physics of the Earth and Planetary Interiors*, **111**, 3–20.
- St. Pierre, M. G., 1996. On the locale nature of turbulence in the Earth's outer core, *Geophysical and Astrophysical Fluid Dynamics*, **83**.
- Stellmach, S. & Hansen, U., 2004. Cartesian convection driven dynamos at low Ekman number, *Physical Review E*, **70**(5), 056312–+.
- Strassmeier, K. G., 2002. Doppler images of starspots, *Astronomische Nachrichten*, **323**, 309–316.
- Strassmeier, K. G., 2006. Doppler Imaging of Rapidly-Rotating M Stars, *Astrophysics and Space Science*, pp. 35–+.
- Weiss, N. O., 1990. Magnetohydrodynamics of sunspots, in *IAU Symp. 142: Basic Plasma Processes on the Sun*, pp. 139–147.
- Weiss, N. O., Thomas, J. H., Brummell, N. H., & Tobias, S. M., 2004. The Origin of Penumbral Structure in Sunspots: Downward Pumping of Magnetic Flux, *Astrophysical Journal*, **600**, 1073–1090.
- Zhang, K. & Jones, C. A., 1994. Convective motions in the Earth's fluid core, *Geophys. Res. Lett.*, **21**, 1939–1942.
- Ziegler, U., 1998. NIRVANA+: An adaptive mesh code for compressible MHD, *Comp. Phys. Comm.*, **109**, 111.
- Ziegler, U., 1999. A Cartesian adaptive mesh code for compressible MHD, *Comp. Phys. Comm.*, **116**, 65.
- Ziegler, U., 2002. Box simulations of rotating magnetoconvection. Spatiotemporal evolution, *Astronomy and Astrophysics*, **386**, 331–346.